DOI: 10.1039/C2CP40493A (Paper) *Phys. Chem. Chem. Phys.*, 2012, **14**, 6569-6576

Investigation of $LiAlH_4$–THF formation by direct hydrogenation of catalyzed Al and LiH

David Lacina [a], **Liu Yang** [a], **Irinder Chopra** [b], **James Muckerman** [a], **Yves Chabal** [b] **and J Graetz** *[a]

[a] *Brookhaven National Laboratory, Upton, NY 11973*

[b] *University of Texas at Dallas, Richardson, TX 75080*

Received 16th February 2012 , Accepted 12th March 2012

First published on the web 13th March 2012

The formation of $LiAlH_4$–THF by direct hydrogenation of Al and LiH in tetrahydrofuran (THF) was investigated using spectroscopic and computational methods. The molecular structures and free energies of the various possible adducts (THF–AlH_3, THF–LiH and THF–$LiAlH_4$) present in a $LiAlH_4$/THF solution were calculated and the dominant species were determined to be contact ion pairs where three THF molecules coordinate the lithium. Raman and X-ray absorption spectroscopy were used to investigate the effect of different Ti precursors on the formation of Al–H species and $LiAlH_4$–THF and determine the optimal reaction conditions. A unique sample stage was developed from a microfluidic cell to evaluate the catalysts *in situ*. The effectiveness of two types of catalysts, titanium chloride ($TiCl_3$) and titanium butoxide ($Ti(C_4H_9O)_4$), and the catalyst concentration were evaluated under similar reaction conditions. Both catalysts were effective at facilitating hydrogenation, although $TiCl_3$ was more effective over the first few cycles with the greatest kinetic enhancement achieved with a low concentration of around 0.15 mol%. These results were qualitatively supported by infrared spectroscopy, which indicated that although a small amount of Ti is necessary for disassociating H_2, excess surface Ti (>0.1 ML) hinders the formation of Al–H species.

1. Introduction

Aluminum hydride (AlH_3) and lithium aluminum hydride ($LiAlH_4$) are a pair of solid metastable hydrides that have received great interest in recent years for the storage and release of hydrogen in mobile energy applications. These materials are particularly well suited for hydrogen storage due to their high gravimetric capacity (8–10%), low hydrogen release temperature (100 °C), and low decomposition enthalpy at room temperature.[1,2] However, these materials are seldom used for hydrogen storage purposes due to the difficulty in re-hydrogenating the spent material after hydrogen release. $LiAlH_4$ has never been completely rehydrogenated directly from LiH and Al, although a small amount of $LiAlH_4$ was formed by ball milling at room temperature.[3] Similarly, thermodynamic studies on AlH_3 indicate that direct hydrogenation of Al only occurs at extremely high pressures (>7 kbar at 300 K).[4] Recently there has been much interest in developing regeneration procedures to reform the metastable hydrides (*e.g.*, $LiAlH_4$

$$LiH + Al^* + 3/2H_2 \leftrightarrow LiAlH_4\text{-}n\text{THF} \rightarrow LiAlH_4 + n\text{THF}\uparrow \quad (1)$$

The presence of Ti is essential for hydrogenation of Al-based metastable hydrides and most alanates[6,7,10,11] at reasonable pressures. Several studies have investigated the kinetic effect of Ti on H_2 desorption[12–14] and the specific surface mechanisms at work,[10,11,15–19] but the role of Ti upon hydrogenation remains unclear. A study by Bogdanovic and Schwickardi[20] originally demonstrated $NaAlH_4$ formation from NaH and Al only when a Ti catalyst was added to the hydrogenation reaction. The presence of a transition metal is known to catalyze the release of hydrog lowering the activation energy barrier,[19] and therefore the Ti plays the dual role of facilitating both the uptal release of hydrogen.[16]

Although the basic procedures (*e.g.*, reaction (1)) to regenerate AlH_3 and $LiAlH_4$ from spent Al have been developed,[7–9] problems related to the Ti catalyst remain. The reduced activation energy barrier from the presence of Ti results in decomposition of the hydride during the separation of the adduct, making it difficult to recover the pure hydride. In an optimal regeneration procedure, the Ti catalyst is removed prior to adduct separation to eliminate the associated stability problems. This requires a better understanding of where the catalyst is located before and after the reaction, the effect of the catalyst precursor during reaction, and the minimum concentration of catalyst needed for hydrogenation. These issues are important for several reasons. First, the location of the Ti after hydrogenation (whether it is associated with the hydride adduct or the unreacted Al) will determine how easily it can be separated from the adduct. Second, establishing a relationship between the catalyst concentration and the reaction rate and yield will help determine the minimum amount of catalyst needed for hydrogenation without reducing the reaction rate. Finally, a commercial regeneration process requires an inexpensive, but effective Ti precursor for the hydrogenation, which is determined through testing different precursors under similar conditions.

In this study the hydrogenation of LiH, THF and catalyzed Al was investigated to (i) determine molecular structure of the hydride adduct, (ii) identify the location of the Ti catalyst (before and after hydrogenation) and (iii) determine the effect of the catalyst type ($TiCl_3$ or Ti butoxide) and concentration on the hydrogenation kinetics. Computations of the molecular structures of relevant species in solution were performed to better understand these hydrogenation reactions. Fig. 1 shows different possible structures of LiH–THF, AlH_3–THF and $LiAlH_4$–THF complexes. These solutes can coordinate with different numbers of THF molecules in THF solution. Absolute free energies of these complexes were calculated in order to determine which species are formed during the reaction. The hydrogenation kinetics of $LiAlH_4$ as a function of Ti concentration was characterized *via* Raman spectroscopy combined with a unique microfluidic system designed to measure the hydride concentration *in situ* as a function of time. X-ray absorption spectroscopy (XAS) and the extended X-ray absorption fine structure (EXAFS) were used to determine the location and local atomic structure of the Ti catalyst before and after hydrogenation.

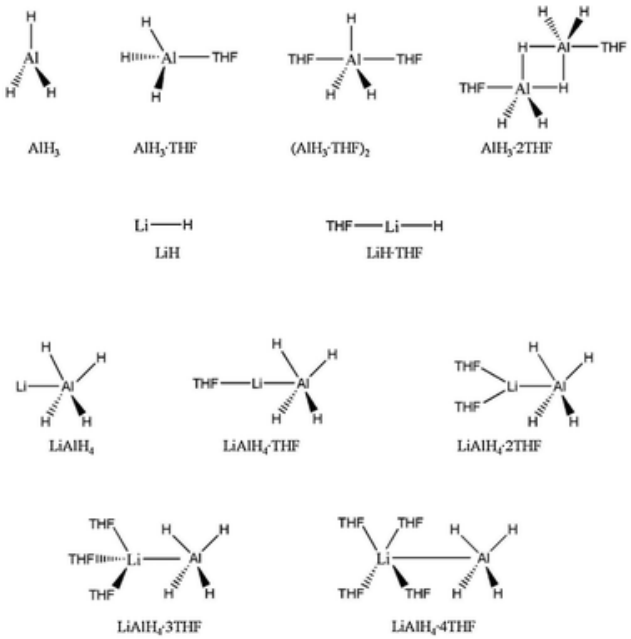

Fig. 1 Different possible structures of THF–AlH_3, THF–LiH and THF–$LiAlH_4$ complexes in THF solution.

2. Experimental section

2.1 Materials

The following materials were obtained from Sigma-Aldrich: tetrahydrofuran (99.9% anhydrous), diethyl ether (99.7% anhydrous), $AlCl_3$ (99.999%), $LiAlH_4$ (reagent grade 95%), $TiCl_3$ (99.995% trace materials basis), liquid $Ti(C_4H_9O)_4$ (reagent grade 97%); from Praxair: hydrogen (99.95%).

The Ti catalyzed Al was prepared in two ways, using precursors of $TiCl_3$ (Al*) and titanium butoxide (Al**). In the first method, aluminum hydride was prepared by the standard ethereal method of Brower *et al.*[21] $TiCl_3$ was added to the alane etherate solution during the synthesis and dissolved, described elsewhere.[5] The alane etherate was dried and decomposed to remove the ether and hydrogen, producing aluminum powder with atomically well-dispersed Ti.[22] Although the 2 mol% Ti was added to solution, much of the Ti is removed during the filtration step and the final Ti concentration was 0.2–0.5 mol% based on a series of ICP-MS/ICP-OES measurements on similar samples. Powder X-ray diffraction performed on the Al* samples revealed only Al metal. No Ti containing species were detected by XRD, likely due to the low final concentration (0.2–0.5 mol%) and poor crystallinity.

The second batch of Ti catalyzed aluminum was prepared by first synthesizing pure AlH_3 (using the Brower method with no $TiCl_3$) and then decomposing the product at 100 °C to produce pure Al powder (confirmed by XRD). Liquid titanium butoxide, $Ti(OBu)_4$, was introduce into the reactor, along with the other precursors (THF, Al and LiH), before initiating the hydrogenation reaction. The uncycled XAS sample was prepared by adding 2 mol% Ti butoxide to Al powder in diethyl ether while mixing with a magnetic stirrer for 30 min and the solid was recovered by filtration. A summary of the various catalyzed Al samples, identifying precursor type, starting concentration and final concentration, is shown in Table 1.

Table 1 Identification of precursor materials and associated concentrations

Material Type	Dopant	Start Concentration	Estimated Final Concentration
High Concentration Al*	$TiCl_3$	2 mol (%)	0.4 mol (%)
Low Concentration Al*	$TiCl_3$	0.5 mol (%)	0.2 mol (%)
2 mol% Al**	$Ti(OBu)_4$	2 mol (%)	2 mol (%)
0.5 mol% Al**	$Ti(OBu)_4$	0.5 mol (%)	0.5 mol (%)
0.15 mol% Al**	$Ti(OBu)_4$	0.15 mol (%)	0.15 mol (%)

2.2 Methods

Hydrogenation reactions were performed in a 300 ml stainless-steel stirred reactor connected to a calibrated gas/vacuum manifold, which was loaded and unloaded in an Argon glovebox. The reactor was charged with 0.6 g of LiH, 90 ml of THF, 1 g of Al* (0.037 mol), or 1 g of pure Al plus liquid Ti butoxide (0.25 ml, 2 mol% Al**; 0.0629 ml, 0.5 mol% Al**; 0.0188 ml, 0.15 mol% Al**). Specifics regarding the formation reactions employing Ti catalyzed Al in this reactor system can be found in other publications.[6,7]

For Raman spectroscopy experiments employing Al**, the Ti catalyzed Al was pre-activated with one formation/decomposition cycle unless specifically stated otherwise. Pre-activation included hydrogenation in a reactor pressurized to 1000 psi at room temperature to allow for nearly complete formation of $LiAlH_4$ over a period of 48 h. After hydrogenation, the reactor was evacuated and heated to 85 °C to decompose the $LiAlH_4$ to base components (LiH, Al and H_2).

A microfluidic cell was developed to evaluate the formation of $LiAlH_4$ in real time and a schematic is shown in Fig. 2.The microfluidic cell was connected to a 300 ml stainless-steel stirred reactor and a gas manifold. In this system the contents of the reactor (a slurry of THF, LiH and catalyzed Al) flowed through the transparent cell, which allowed Raman spectra to be acquired throughout the hydrogenation reaction without exposing the contents to air. The reactor was pressurized to 30 psi H_2 and the slurry was agitated to ensure dissolution of H_2 in the liquid. The liquid contents of the reactor were passed through the liquid cell at regular intervals and Raman spectra were acquired until the reaction was complete. The internal temperature of the reactor (gas and liquid) and manifold (kept at room temperature) were recorded using Type K thermocouples. Upon completion, the reactor was returned to the glovebox and the solids were filtered from the liquid using a 0.7 μm glass fiber filter combined with a diatomite filter aid. Samples used in the XAS studies were prepared under the same conditions.

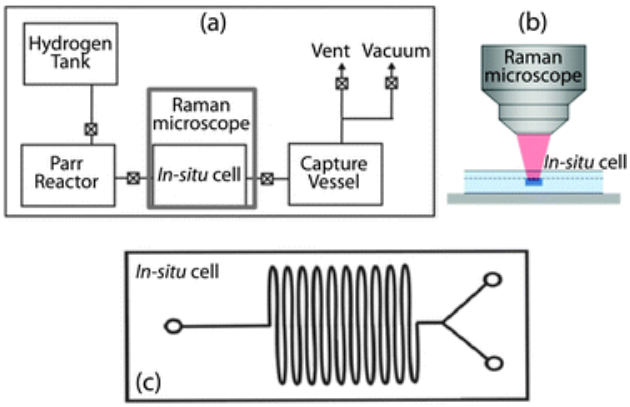

Fig. 2 (a) Schematic of *in situ* Raman and microfluidic system where (b) the confocal Raman microscope is used

Experiments were also performed on single crystal Al(111) surfaces to investigate the chemisorption of atomic hydrogen and the formation of alanes as a function of Ti coverage. Using an experimental set up described in previous work,[16,19] an Al(111) surface was first doped with low coverages of Ti (0.1 ML, 0.2 ML, 0.3 ML) and then exposed to a low atomic hydrogen flux (3×10^{15} H/cm^2). Alane formation was observed on both clean and Ti-doped Al(111) surfaces, although the concentration and structure is a function of Ti coverage as described below.

Raman spectroscopy was carried out using a Witec Alpha 300 confocal Raman microscope utilizing a neodymium-doped yttrium aluminum garnet (Nd:YAG) laser with an excitation wavelength of 532 nm, a 20 objective, and a 38.6 μm spot size. The resolution of the microscope was 3 cm^{-1}. Ti K-edge spectra were co beamline X-3B at the National Synchrotron Light Source. Spectra were recorded in fluorescence yield mod 13-element Ge detector with an energy resolution of 3 eV for all samples. Studies were performed with the sample holder in a chamber under vacuum and oriented at 45° to the incident X-ray beam. All samples were loaded in a glove box and sealed in a sample holder under argon. Due to the low Ti concentration in these materials, the spectra were not corrected for self absorption.

2.3 Theoretical calculations

All computations were carried out with the Gaussian09 suite of programs[23] using the B3LYP hybrid density functional method.[24] All-electron basis sets were employed at the B3LYP/6-31+G(d,p)[25–27] level of theory. Optimized geometries in the gas phase were re-optimized in a CPCM[28–30] treatment of the THF solvent using UAHF radii. The absolute free energy of a solute in THF solution is calculated as $G^*_{(s)} = G^\circ_{(g)} + \Delta G^{\circ\to *} + \Delta G^*_S$ where ΔG^*_S is the solvation free energy. The standard state correction $(\Delta G^{\circ\to *} = 1/894\ \text{kcal/mol})$ is included due to the change from the quantum chemical standard state of an ideal gas in the gas phase (1 atm) to the experimental standard state in solution (1 mol l^{-1}). In order to calculate the absolute free energy of a THF molecule in THF solution, the "self-solvation free energy", which is the free energy associated with moving the gas phase molecule at 1 mol l^{-1} to the pure liquid phase, needs to be calculated. The "self-solvation energy" of THF is −4.297 kcal mol^{-1}, which can be calculated using $\Delta G^*_{\text{self}} = -RT\ln(10)\log(\frac{M_{liq}/M^\circ}{P_{vapor}/P^\circ})$. Here M° is equal to 1 mol l^{-1}, P° is the pressure (24.45 atm) of an ideal gas at 1 M concentration and 298 K, and M_{liq} is 12.33 mol l^{-1}, which is the molarity of THF in its pure liquid form. It can be calculated using: $M_{liq} = \rho_{liq}/MW_{liq}$. The absolute free energy of THF in its liquid phase is then equal to $G^*_{(liq)} = G^\circ_{(g)} + \Delta G^{\circ\to *} + \Delta G^*_{\text{self}}$.

3 Results and discussion

3.1 Theory

Different molecular structures of LiH, AlH_3 and $LiAlH_4$ in THF solution were examined and their absolute free energies are listed in Table 2. Different numbers of solvent THF molecules were included to balance the total number of THF molecules in each complex. The most stable structures of each complex are shown in Fig. 3. The re-optimized structures of these species in THF solution all have larger Li–Al distance than that of isolated molecules in the gas phase. This indicates a significant polarization in the THF solution since the polarized continuum model stabilizes charge separation.

Table 2 Relative free energy of different configurations of LiH, AlH_3 and $LiAlH_4$ in THF solution. Different numbers of solvent THF molecules were included to balance the total number of THF molecules

Species	Free energy in THF solution (kcal mol^{-1})
$AlH_3 \cdot THF_{(s)} + THF_{(liq)}$	−19.12
$½(AlH_3 \cdot THF)_{2(s)} + THF_{(liq)}$	−15.10
$AlH_3 \cdot 2THF_{(s)}$	−15.29
$LiH_{(s)} + THF_{(liq)}$	0
$LiH \cdot THF_{(s)}$	−4.184
$LiAlH_{4(S)} + 4THF_{(liq)}$	0
$LiAlH_4 \cdot THF_{(s)} + 3THF_{(liq)}$	−2.886
$LiAlH_4 \cdot 2THF_{(s)} + 2THF_{(liq)}$	−0.982
$LiAlH_4 \cdot 3THF_{(s)} + THF_{(liq)}$	−3.376
$LiAlH_4 \cdot 4THF_{(s)}$	3.422

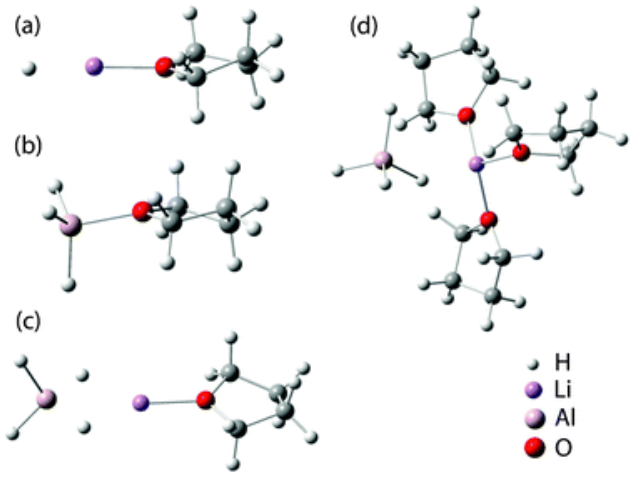

Fig. 3 Optimized geometries of the most stable configuration of (a) LiH·THF, (b) AlH_3·THF, (c) $LiAlH_4$·THF, and (d) $LiAlH_4$·3THF in THF solution.

The results indicate that LiH and AlH_3 both prefer to coordinate with one THF molecule. The interaction between the metal atom and the oxygen atom in THF stabilizes the complexes. The computed absolute free energies of different solvated $LiAlH_4$ complexes show two minima. $LiAlH_4$ coordinates with one THF with a Li–Al distance of 2.78 Å (Fig. 3c). If the Li–Al distance increases to 3.42 Å, $LiAlH_4$ can coordinate with three THF molecules (Fig. 3d). The free energy of $LiAlH_4$·THF is only 0.49 kcal mol^{-1} higher (Table 1) than $LiAlH_4$·3THF, and both configurations are contact ion pairs in which the $LiAlH_4$ coordinates strongly with THF molecules. As the Li–Al distance increases, more THF molecules are able to coordinate with Li. $LiAlH_4$ can coordinate with four THF molecules ($LiAlH_4$·4THF) and form solvent-separated ion pairs at a Li–Al distance of 5.71 Å. However, the absolute free energy of this structure is about 6.8 kcal mol^{-1} higher than that of $LiAlH_4$·3THF. Different from the tetrahedral geometry in THF solution, $LiAlH_4$·4THF in the gas phase forms a trigonal bypyramidal structure, coordinating with four THF molecules and a hydrogen atom. This kind of geometrical change is not observed in other species.

We can conclude that at room temperature, the predominant species of $LiAlH_4$ in THF solution are the contact ion

dissociation process of $LiAlH_4$ which is a three-THF coordinated configuration and it corresponds to the contact ion pair.

Given the free energy of these associated species, the reaction $LiH_{(s)} + AlH_{3(s)} \rightarrow LiAlH_{4(s)}$ in THF solution becomes $LiH{\cdot}THF_{(s)} + AlH_3{\cdot}THF_{(s)} + THF_{(liq)} \rightarrow LiAlH_4{\cdot}3THF_{(s)}$ with a reaction free energy of −16.41 kcal mol^{-1}.

3.2 Raman and infrared spectroscopy

The intensity of the Al–H stretch mode in the Raman spectrum, collected during the formation of $LiAlH_4$, was used to determine the rate of formation and product yield as a function of Ti concentration. Pure solid lithium alu hydride has two strong Raman peaks of interest, at 1760 cm^{-1} and 1835 cm^{-1}, that could potentially be used the formation of $LiAlH_4$, but the focus will be on the former peak as the latter is not visible for THF solvate $LiAlH_4$. All of the Raman spectra were normalized to the intensity of the major THF peaks after background subtraction and the integrated intensity of the Al–H stretch peak was used to quantify the concentration of $LiAlH_4$ at various stages of the reaction. Since the experimental procedures were the same for all samples, this empirical relationship was also used to compare the rate and total yield of $LiAlH_4$ using different Ti precursors and concentrations.

Raman spectra were acquired during the formation of $LiAlH_4$ (reaction (1)) using two concentrations of the $TiCl_3$ catalyst (0.2 mol% and 0.4 mol%). The Raman spectra obtained for $LiAlH_4$ formed with 0.4 mol% Ti are shown in Fig. 4a (data from 0.2 mol% Ti are not shown). The peaks at 1230 cm^{-1} and 1470 cm^{-1} are associated with CH_2 deformation vibrations from the THF and do not change during the reaction. The Al–H stretch peak at 1760 cm^{-1} showed a similar change over the full reaction for both the high and low concentrations, suggesting a similar reaction rate and yield. This is confirmed by the integrated intensity of the 1760 cm^{-1} Al–H peaks as a function of time shown in Fig. 5. The final yield in these experiments was determined from the amount of unreacted Al recovered after the reaction was complete (no further hydrogen uptake). A standard of $LiAlH_4$ in THF was prepared at the expected final concentration (0.36 M of $LiAlH_4$ in THF) and the intensity of the Al–H stretch mode in the Raman spectrum was compared with the experimental results (top spectrum in Fig. 4). The results from this experiment indicate the effectiveness of the Ti catalyst saturates at or below the starting concentration of 0.5 mol% (for $TiCl_3$).

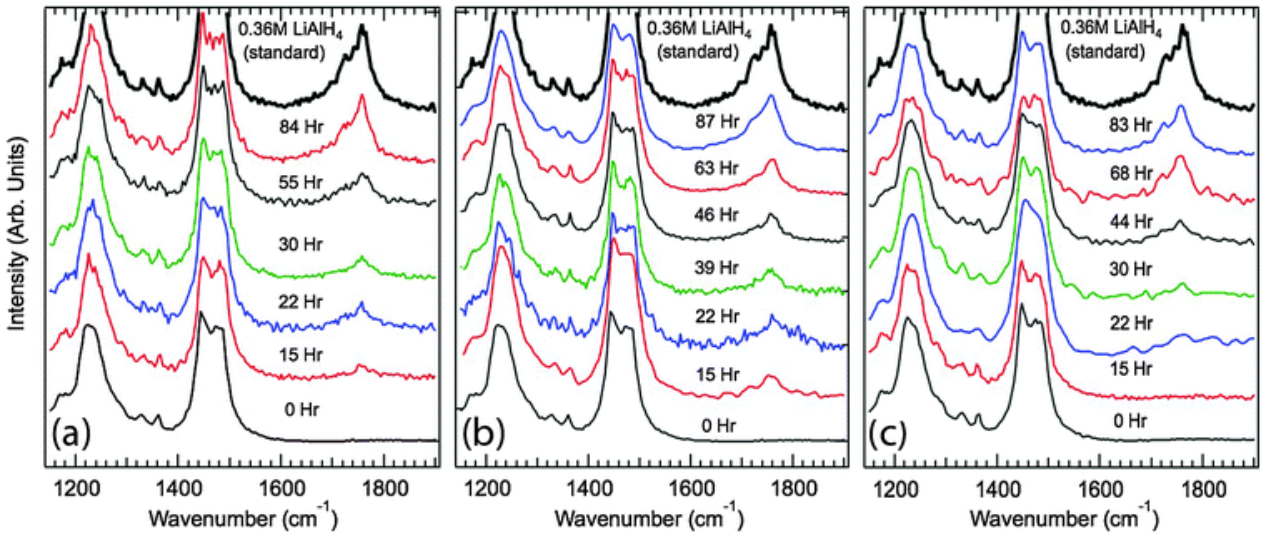

Fig. 4 Raman spectra collected during the formation of $LiAlH_4$–THF (reaction (1)) at different times using (a) 0.4

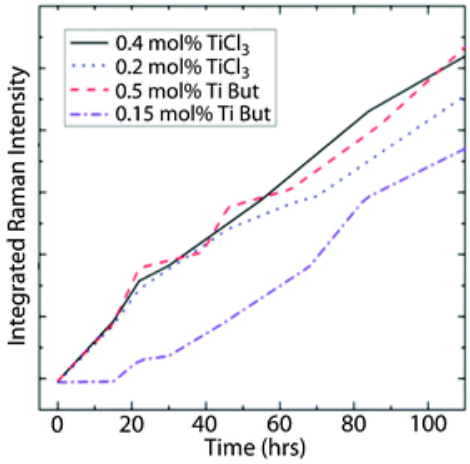

Fig. 5 Integrated intensities of the 1760 cm^{-1} peak data from Fig. 4 showing high concentration (2 mol% $TiCl_3$), 0.5 mol% $TiCl_3$, 0.5 mol% Ti butoxide, 0.15 mol% Ti butoxide.

The formation of $LiAlH_4$ using Al** was studied to determine the effectiveness of the Ti butoxide precursor with respect to $TiCl_3$. In contrast with $TiCl_3$, the liquid Ti butoxide is added directly to the Al powder allowing for precise control over the final Ti concentration since no Ti is lost during filtration. The Al** samples used in the Raman experiments were pre-activated with two complete formation/decomposition cycles.

Fig. 4b and c show results from the Al** experiments at 0.5 mol% and 0.15 mol%, respectively. The 0.5 mol% Al** formation rate and yield are the same as that determined for the high and low concentration Al*, as shown in Fig. 5, which suggests the catalyst reaches a saturation at some point below 0.5 mol% . The 0.15 mol% experiment, shown in Fig. 4c, demonstrates a slower formation rate and a reduced final yield when compared to higher concentrations, which can also be seen in Fig. 5.

Infrared spectroscopy was used to determine the rate of Al–H formation as function of Ti coverage (*i.e.*, surface concentration) on Ti-doped single crystal Al(111) surfaces. Upon low atomic hydrogen exposures, the concentration of AlH_3 chemisorbed at step edges clearly decreases as a function of Ti coverage, as shown in Fig. 6. The intensity of the AlH_3 stretch mode at 1790 cm^{-1} is at a maximum for 0.1 ML Ti (10% of a monolayer) and decreases for 0.2 ML Ti coverage and is almost nonexistent for the 0.3 ML Ti coverage. Since the concentration of AlH_3 reflects the ability of atomic hydrogen to diffuse and form alanes at steps,[16] the reduction in the formation of chemisorbed alanes can be explained by the decrease in H and Al adatom diffusion on Al(111) planes due to the presence of Ti. Formation of the $TiAl_3$ like configurations suggests that Ti doping results in strengthening the surface bonds, thereby preventing the formation and migration of Al adatoms. These results indicate that although the presence of Ti is necessary to split the molecular H_2, once atomic H has formed the Ti can hinder the formation of Al–H species. Therefore the optimal Al surface consists of sparsely distributed Ti (0.1 ML). This is supported by the recent work of Liu *et al.*, that showed a decrease in the yield of $LiAlH_4$ with catalyst loading above ~0.2 mol%.[32]

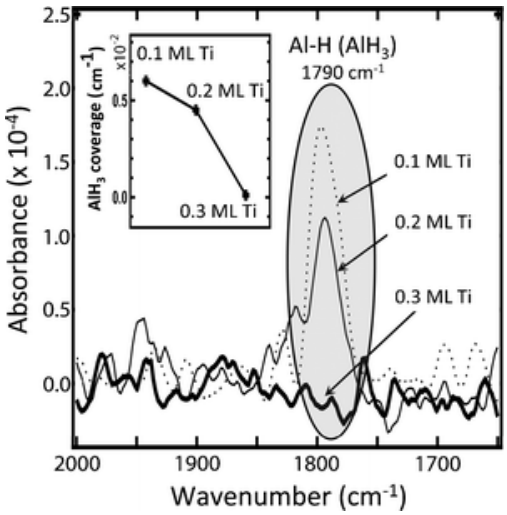

Fig. 6 Infrared absorbance spectra obtained after Al(111) surface at 90 K is exposed to atomic hydrogen (3×10^{15} H/cm^2). At such low exposures, AlH_3 is chemisorbed on the Al(111) step edges with a distinct absorbance feature at 1790 cm^{-1} (terminal hydrogen—Al–H—stretch). Increasing Ti coverages reduce alane formation (almost non-existent for 0.3 ML Ti coverage). The inset plots the change in the integrated intensities of chemisorbed alanes as a function of Ti coverage.

3.3 X-ray absorption spectroscopy

Previous studies have examined the location of Ti in $NaAlH_4$ and TEDA-alane using nuclear magnetic resonance (NMR),[33] XRD,[34,35] and transmission electron microscopy (TEM).[22,36] However, X-ray absorption spectroscopy is one of the best methods for analyzing the Ti catalyst in these materials since it allows for the characterization of the local environment on the surface of the aluminum particles in addition to detecting the presence of Ti in the material itself. The Ti K-edge spectra and the Fourier transform of the k^2-weighted EXAFS data (with phase shift correction) are shown in Fig. 7 for the aluminum precursor (Al*, 0.4 mol% Ti), the $LiAlH_4$ product, and the recovered unreacted solids.

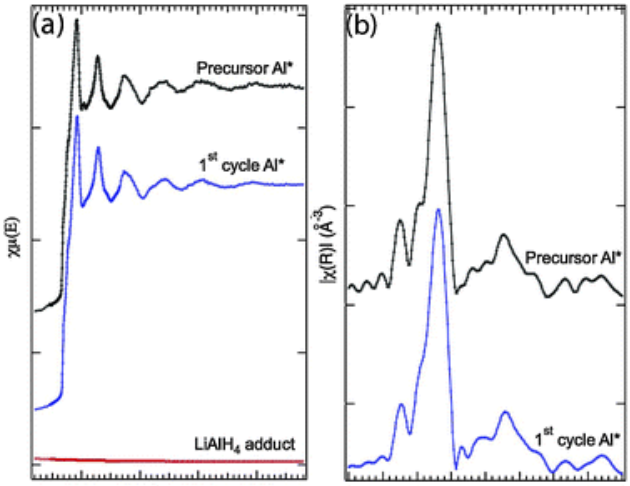

Fig. 7 X-ray absorption spectra from the Al* precursor (0.4 mol% Ti), the unreacted Al, and the $LiAlH_4$ solid adduct showing (a) the Ti K-edges and (b) the Fourier transform of the k^2-weighted EXAFS data with peaks indicating the Ti–Al pairs at ~2.65 Å.

The Ti K-edge onset (4966 eV) and the general shape of the Ti K-edge for both the Al* precursor and the unreacted solids are similar, indicating no change in the local atomic or electronic structure around the Ti d hydrogenation. The k^2-weighted EXAFS data in Fig. 7b illustrates a similar local coordination with the don peak at 2.65 Å, which indicates Ti–Al pairs similar to $TiAl_3$. This conclusion is supported by previous inves on the role of Ti, which showed that when Al* is employed in the formation of $NaAlH_4$, through a ball milling process, the Ti most likely forms Ti–Al clusters with a local structure comparable to disordered $TiAl_3$ nanoclusters exhibiting short range order.[10,11] A qualitative comparison of the Ti K-edge intensities from the starting Al and the unreacted Al (after adduct formation) clearly indicates a higher Ti concentration in the unreacted material, as expected.

The Ti K-edge and EXAFS data for $LiAlH_4$ formed using Al* shows no increase in intensity at the expected Ti K-edge energy (4966 eV), indicating that no detectable titanium is present in the recovered hydride. This is an important finding since it implies that if the hydride is solubilized (or a liquid) then the Ti catalyst is easily separated from the hydride by simply filtering off the unreacted material. These results are similar to those observed for the formation of trimethylamine-alane (TMAA), which also showed the presence of Ti in the unreacted Al, but not the alane adduct.[6] A study by Graham *et al.* found Ti particles in recovered TEDA alane adduct formed using Al*,[22] but it is likely that these particles were associated with unreacted Al* that were not separated from the insoluble adduct after the reaction.

Fig. 8 displays the Ti K-edge and EXAFS data collected from the precursors and products of the Ti butoxide catalyzed Al (Al**), which exhibited a different local Ti atomic environment than the $TiCl_3$ catalyzed (Al*) samples. Three distinct local atomic states are visible in the XAS data in Fig. 8. In the first state, obtained from the uncycled Al**, the Ti K-edge onset contains two peaks (at 4980 eV and 5005 eV) instead of a single peak, which indicates a different local atomic structure around the Ti than what was observed in the Al* samples. The k^2-weighted EXAFS data in Fig. 8b shows a single dominant peak at 1.8 Å, which is consistent with the Ti–O bond lengths (~1.8 Å).[37] This information suggests that liquid Ti butoxide simply coats the Al particles once it is added to the solution and the Ti does not initially form Ti–Al bonds.

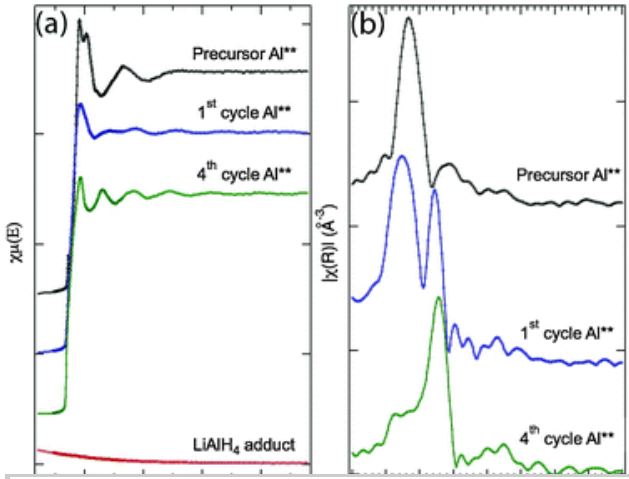

Fig. 8 X-ray absorption spectra from the Al** precursor (2 mol% Ti) after 1 formation cycle, the unreacted Al after 4 formation cycles, and the $LiAlH_4$ solid adduct showing (a) the Ti K-edges and (b) the Fourier transform of the k^2-weighted EXAFS data with peaks indicating the Ti–O (~1.80 Å) and Ti–Al (~2.65 Å) pairs.

After the completion of the first formation step the Ti K-edge has changed, with peaks that more closely the spectra from the $TiCl_3$ doped samples (Fig. 7). The k^2-weighted EXAFS data in Fig. 8b shows two distin at 1.80 Å and 2.65 Å indicating the presence of both Ti–O bonds (~1.80 Å) and Ti–Al bonds (~2.65 Å). Th results indicate that after the first formation cycle, some of the Ti butoxide coated Al has converted into Ti–Al.

After 4 complete cycles, the Ti K-edge spectrum and edge onset, displayed in Fig. 8a, matches the data collected from the $TiCl_3$ (Al*) experiments (Fig. 7). The k^2-weighted EXAFS data shows a single distinct peak at ~2.65 Å, which matches the position for Ti–Al bonding in $TiAl_3$ clusters. This suggests that although Ti butoxide may not be as effective as $TiCl_3$ during the initial hydrogenation cycles, after several cycles the Ti catalyst is effectively the same regardless of precursor type and should support similar reaction rates and yields.

3.4 Broader impacts

Effectiveness, cost, and stability are the three most important factors that determine if a material is a viable hydrogen storage compound for commercial applications. Considering these factors, lithium aluminum hydride ($LiAlH_4$) and aluminum hydride (AlH_3) have great potential as solid-state hydrogen storage materials in comparison with other metastable hydrides.[38,39] A promising method to form $LiAlH_4$ is given in reaction (1) and a similar process can be used to form AlH_3 at low hydrogen pressures, as shown below:

$$Al + 2(C_3H_9N) + 3/2H_2 \rightarrow AlH_3{\cdot}2(C_3H_9N) \quad (2)$$

$$AlH_3{\cdot}2(C_3H_9N) + C_6H_{15}N \rightarrow AlH_3{\cdot}C_6H_{15}N + 2(C_3H_9N)\uparrow \quad (3)$$

$$AlH_3{\cdot}C_6H_{15}N \rightarrow AlH_3 + C_6H_{15}N\uparrow \quad (4)$$

The formation of both $LiAlH_4$ and AlH_3 requires a Ti catalyst at mild hydrogen pressures. The results for $LiAlH_4$ suggest that $TiCl_3$ is a more effective precursor in hydrogenation, but Ti butoxide might be more cost effective commercially since it is less expensive and easier to control the amount of catalyst used in the reaction. Since the hydrogenation mechanism for $LiAlH_4$ and AlH_3 are likely to be similar, we expect the Ti butoxide and $TiCl_3$ catalysts will have a similar behavior in the regeneration procedure for AlH_3. This work, and previous studies, indicate that the Ti catalyst (indpendent of catalyst precursor) remains with the unreacted Al and does not become associated with the adduct. This implies that, regardless of the hydride being formed, the catalyst should be easily removed before adduct separation (*e.g.*, reaction (4)) to prevent hydride decomposition.

Previous work with $NaAlH_4$ suggests that Ti–Al clusters can slowly form a more stable, less active $TiAl_3$ alloy over many cycles.[10,11] The infrared absorbance spectra in Fig. 6 clearly indicate that Ti doping, and the resulting Ti–Al configurations, leads to a strengthening of the surface bonds, thereby preventing the formation and migration of Al adatoms. Applied to the regeneration of AlH_3 or $LiAlH_4$, a single batch of Al would likely experience lower overall hydride yields with each cycle due to the locally higher concentration of Ti and the greater stability of the

Ti–Al over multiple cycles and whether or not the capacity loss can be recovered by the addition of fresh catalyst.

4. Conclusions

The formation of $LiAlH_4$–THF by direct hydrogenation of Al, LiH and THF was investigated using spectroscopic techniques and the molecular structures and free energies of the various possible adducts (THF–AlH_3, THF–LiH and THF–$LiAlH_4$) were determined by computational methods. At room temperature, the predominant species of $LiAlH_4$ in THF solution are the contact ion pairs with a $LiAlH_4$ in a three-THF coordinated configuration. IR spectroscopy on Ti-decorated Al (111) revealed that low Ti coverages (~0.1 ML) are ideal for the formation of surface A species. These results were qualitatively supported by *in situ* Raman measurement made on Ti catalyzed Al powders, which showed the greatest reaction rates at low Ti concentrations (~0.15 mol%). When Ti was int as Ti butoxide, approximately four cycles were necessary to transform the Ti–O bonds into Ti–Al bonds and form a Ti–Al species similar to that formed with $TiCl_3$. These results support the assertion that Ti can promote the formation of alanes and alanates and can be easily separated from the alane or alanate adduct for regeneration. These results also clearly demonstrate that the recovered Ti–Al can be re-used for future hydrogenation reactions, although the rate and yield may decline somewhat with each subsequent cycle.

Acknowledgements

This work was fully supported by the Office of Basic Energy Sciences, U.S. Department of Energy under Contract No. DE-AC02-98CH10886. The authors gratefully acknowledge the National Synchrotron Light Source and the Center for Functional Nanomaterials at Brookhaven National Laboratory for use of beamline X3B and the Raman microscope. Calculations were carried out in large part at the CFN Computational Cluster under a user proposal by JTM.

References

1. J. Graetz and J. J. Reilly, *J. Phys. Chem. B*, 2005, **109**, 22181 CrossRef CAS Search PubMed .
2. J. Graetz, J. J. Reilly, V. A. Yartys, J. P. Maehlen, B. M. Bulychev, V. E. Antonov, B. P. Tarasov and I. E. Gabis, *J. Alloys Compd.*, 2011, **509S**, S517 CrossRef CAS Search PubMed .
3. Y. Kojima, Y. Kawai, T. Haga, M. Matsumoto and A. Koiwai, *J. Alloys Compd.*, 2007, **441**, 189 CrossRef CAS Search PubMed .
4. J. Graetz and J. J. Reilly, *J. Alloys Compd.*, 2006, **424**, 5 CrossRef CAS Search PubMed .
5. J. Graetz, S. Chaudhuri, J. Wegrzyn, Y. Celebi, J. R. Johnson, W. Zhou and J. J. Reilly, *J. Phys. Chem. C*, 2007, **111**, 19148 CAS Search PubMed .
6. D. Lacina, J. Wegrzyn, J. J. Reilly, Y. Celebi and J. Graetz, *Energy Environ. Sci.*, 2010, **3**, 1099 CAS Search PubMed .
7. D. Lacina, J. J. Reilly, Y. Celebi, J. Wegrzyn and J. Graetz, *J. Phys. Chem. C*, 2010, **115**, 3789 Search PubMed .
8. J. Graetz, J. Wegrzyn and J. J. Reilly, *J. Am. Chem. Soc.*, 2008, **130**, 17790 CrossRef CAS Search PubMed .
9. X. F. Liu, G. S. McGrady, H. W. Langmi and C. M. Jensen, *J. Am. Chem. Soc.*, 2009, **131**, 5032 CrossRef CAS Search PubMed .
10. J. Graetz, A. Y. Ignatov, T. A. Tyson, J. J. Reilly and J. Johnson, *Appl. Phys. Lett.*, 2004, **85**, 500 CrossRef CAS Search PubMed .
11. S. Chaudhuri, J. Graetz, A. Ignatov, J. J. Reilly and J. T. Muckerman, *J. Am. Chem. Soc.*, 2006, **128**, 11404 CrossRef CAS Search PubMed .

13. K. Gross and G. Thomas, *J. Alloys Compd.*, 2002, **339**, 299 CrossRef CAS Search PubMed .
14. C. P. Balde′, O. Leynaud, P. Barnes, E. Pelaez-Jimenez, K. de Jong and J. Bitter, *Chem. Commun.*, 2011, **47**, 2143 RSC .
15. Y. Song, J. H. Dai, X. M. Liang and R. Yang, *Phys. Chem. Chem. Phys.*, 2010, **12**, 10942 RSC .
16. I. S. Chopra, S. Chaudhuri, J.-F. Veyan, J. Graetz and Y. J. Chabal, *J. Phys. Chem. C*, 2011, **115**, 16701 CAS Search PubMed .
17. Y. Wang, F. Zhang, R. Stumpf, P. Lin and M. Y. Chou, *Phys. Rev. B: Condens. Matter Mater. Phys.*, 2011, **83**, 195419 CrossRef CAS Search PubMed .
18. S. Chaudhuri and J. T. Muckerman, *J. Phys. Chem. B*, 2005, **109**, 6952 CrossRef CAS Search PubMed .
19. I. S. Chopra, S. Chaudhuri, J. F. Vevan and Y. J. Chabal, *Nat. Mater.*, 2011, **10**, 884 CrossRef CAS Search PubMed .
20. B. Bogdanovic and M. Schwickardi, *J. Alloys Compd.*, 1997, **253**, 1 CrossRef CAS Search PubMed .
21. F. M. Brower, N. E. Matzek, P. F. Reigler, H. W. Rinn, C. B. Roberts, D. L. Schmidt, J. A. Snover and K. Terada, *J. Am. Chem. Soc.*, 1976, **98**, 2450 CrossRef CAS Search PubMed .
22. D. D. Graham, J. Graetz, J. Reilly, J. Wegrzyn and I. Robertson, *J. Phys. Chem. C*, 2010, **114**, 15207 CAS Search PubMed .
23. M. J. Frisch, G. W. Trucks, H. B. Schlegel, G. E. Scuseria, M. A. Robb, J. R. Cheeseman, G. Scalmani, V. Barone, B. Mennucci, G. A. Petersson, H. Nakatsuji, M. Caricato, X. Li, H. P. Hratchian, A. F. Izmaylov, J. Bloino, G. Zheng, J. L. Sonnenberg, M. Hada, M. Ehara, K. Toyota, R. Fukuda, J. Hasegawa, M. Ishida, T. Nakajima, Y. Honda, O. Kitao, H. Nakai, T. Vreven, J. A. Montgomery, Jr., J. E. Peralta, F. Ogliaro, M. Bearpark, J. J. Heyd, E. Brothers, K. N. Kudin, V. N. Staroverov, R. Kobayashi, J. Normand, K. Raghavachari, A. Rendell, J. C. Burant, S. S. Iyengar, J. Tomasi, M. Cossi, N. Rega, J. M. Millam, M. Klene, J. E. Knox, J. B. Cross, V. Bakken, C. Adamo, J. Jaramillo, R. Gomperts, R. E. Stratmann, O. Yazyev, A. J. Austin, R. Cammi, C. Pomelli, J. W. Ochterski, R. L. Martin, K. Morokuma, V. G. Zakrzewski, G. A. Voth, P. Salvador, J. J. Dannenberg, S. Dapprich, A. D. Daniels, Ö. Farkas, J. B. Foresman, J. V. Ortiz, J. Cioslowski and D. J. Fox, *Gaussian 09, Revision A.1*, Gaussian, Inc., Wallingford CT, 2009 Search PubMed .
24. A. D. Becke, *J. Chem. Phys.*, 1993, **98**, 5648 CrossRef CAS Search PubMed .
25. R. Ditchfie, W. J. Hehre and J. A. Pople, *J. Chem. Phys.*, 1971, **54**, 724 CrossRef CAS Search PubMed .
26. M. M. Francl, W. J. Pietro, W. J. Hehre, J. S. Binkley, M. S. Gordon, D. J. Defrees and J. A. Pople, *J. Chem. Phys.*, 1982, **77**, 3654 CrossRef CAS Search PubMed .
27. W. J. Hehre, R. Ditchfie and J. A. Pople, *J. Chem. Phys.*, 1972, **56**, 2257 CrossRef CAS Search PubMed .
28. A. Klamt and G. Schuurmann, *J. Chem. Soc., Perkin Trans. 2*, 1993, 799 RSC .
29. V. Barone and M. Cossi, *J. Phys. Chem. A*, 1998, **102**, 1995 CrossRef CAS Search PubMed .
30. M. Cossi, N. Rega, G. Scalmani and V. Barone, *J. Comput. Chem.*, 2003, **24**, 669 CrossRef CAS Search PubMed .
31. D. E. Bikiel, F. Di Salvo, M. C. G. Lebrero, F. Doctorovich and D. A. Estrin, *Inorg. Chem.*, 2005, **44**, 5286 CrossRef CAS Search PubMed .
32. X. Liu, H. W. Langmi, S. D. Beattie, F. F. Azenwi, G. S. McGrady and C. M. Jensen, *J. Am. Chem. Soc.*, 2011, **133**, 15593 CrossRef CAS Search PubMed .
33. T. Ivancic, S.-J. Hwang, R. Bowman, D. Birkmire, C. M. Jensen, T. Udovic and M. S. Conradi, *J. Phys. Chem. Lett.*, 2010, **1**, 2412 CrossRef CAS Search PubMed .
34. A. G. Haiduc, H. A. Stil, M. A. Schwarz, P. Paulus and J. J. C. Geerlings, *J. Alloys Compd.*, 2005, **393**, 252 CrossRef CAS Search PubMed .

E. H. Majzoub, J. L. Herberg, R. Stumpf, S. Spangler and R. S. Maxwell, *J. Alloys Compd.*, 2005, **394**,

281 CrossRef CAS Search PubMed .
37. D. M. Pickup, G. Mountjoy, G. W. Wallidge, R. Anderson, J. M. Cole, R. J. Newport and M. E. Smith, *J. Mater. Chem.*, 1999, **9**, 1299 RSC .
38. J. Graetz, *Chem. Soc. Rev.*, 2009, **38**, 73 RSC .
39. J. Graetz and J. J. Reilly, *Scr. Mater.*, 2007, **56**, 835 CrossRef CAS Search PubMed .